Averaged variational principle for autoresonant Bernstein–Greene–Kruskal modes

P. Khain and L. Friedland[a)]
Racah Institute of Physics, Hebrew University of Jerusalem, Jerusalem 91904, Israel

(Received 26 May 2010; accepted 21 September 2010; published online 26 October 2010)

Whitham's averaged variational principle is applied in studying dynamics of formation of autoresonant (continuously phase-locked) Bernstein–Greene–Kruskal (BGK) modes in a plasma driven by a chirped frequency ponderomotive wave. A flat-top electron velocity distribution is used as a model allowing a variational formulation within the water bag theory. The corresponding Lagrangian, averaged over the fast phase variable yields evolution equations for the slow field variables, allows uniform description of all stages of excitation of driven-chirped BGK modes, and predicts modulational stability of these nonlinear phase-space structures. Numerical solutions of the system of slow variational equations are in good agreement with Vlasov–Poisson simulations.
 [doi:10.1063/1.3500246]

I. INTRODUCTION

Excitation and control of large amplitude plasma waves is an important goal of plasma research. For example, such waves can be used for charged particle acceleration[1] or pulse amplification via Raman scattering.[2] The plasma waves [e.g., Trivelpiece–Gould modes[3]] are easily generated and stable in cases when their phase velocity is in the tail of the velocity distribution of the plasma species. However, when the wave resonates with the bulk of the distribution, it is strongly Landau damped.[4] At first glance this damping seemed unavoidable, so it was quite surprising when Bernstein, Greene, and Kruskal[5] (BGK) in 1957 predicted the existence of a large class of undamped kinetic plasma waves (BGK modes) in collisionless plasmas. According to their theory, a specific BGK mode would only be dissipationless for an appropriate velocity distribution, which is delicately shaped in the kinetic resonance region.

After more than five decades of studies, a controlled generation of large amplitude BGK modes in experiments has proven difficult. Following the prediction of O'Neil[6] that Landau damped waves may evolve into a BGK equilibrium, a natural path to excitation of BGK modes used a strong perturbation-relaxation approach.[7–9] Alternatively, BGK modes may emerge due to instabilities.[10,11] This passive self-organization is sensitive to initial conditions and may involve a violent stage, leading to poor controllability of the excited BGK structures.

Recently, a different approach to excitation of BGK modes was suggested involving driving the plasma by a chirped frequency perturbation passing through kinetic resonances. The idea was first implemented in non-neutral plasmas; see Refs. 12–14, using the bounce-type resonance. A similar approach was suggested in quasineutral plasmas[15] via the Cherenkov resonance. It involved driving a flat-top distribution of the plasma electrons by a ponderomotive wave having slowly varying frequency. The phase velocity of the drive was outside the electron velocity distribution initially. A gradual decrease of the driving frequency resulted in passage through the fluid resonance in the plasma followed by successive Cherenkov resonances with different parts of the electron distribution function. As a result, stable voids (holes) in phase space were formed, as illustrated in Fig. 1 in Sec. II. These holes were phase-locked to the drive and the electrostatic field associated with the holes comprised a continuously phase-locked (autoresonant) BGK mode in the plasma. An attempt of formulating the theory of these coherent structures in Ref. 15 used either fluid or kinetic descriptions in different stages of excitation. The theory of Ref. 15 was followed by the development of an adiabatic water bag model of autoresonant phase-space holes in Ref. 16, yielding a uniform description of all stages of evolution shown in Fig. 1. The new theory assumed a flat distribution of electrons in phase space confined between evolving sharp boundaries (limiting trajectories). Due to the incompressibility of the phase-space fluid, the understanding of the dynamics of the limiting trajectories was sufficient for describing the evolution of the entire distribution. The use of the adiabatic invariants (actions of the limiting trajectories) simplified the problem and allowed calculation of the electric field associated with the BGK mode. The theory was also generalized to arbitrary initial distributions via a multiwater bag theory. Nevertheless, the formalism in Ref. 16 assumed a continuing *ideal* phase-locking (zero phase mismatch) between the BGK mode and the drive, which is only valid in the limit of very small driving frequency chirp rates. Furthermore, the theory described a slowly evolving quasisteady state of the driven wave, but did not address the numerically observed stability of the chirped-driven BGK structures.

In the present work we fill the missing gaps of the aforementioned studies and develop a complete, self-consistent adiabatic theory of driven autoresonant BGK modes using the Whitham's averaged variational principle.[17] The application of this approach in the case of interest is justified, as long as the time scales of variation of the electric field amplitude and frequency of the driven kinetic structures are

[a)]Electronic mail: lazar@vms.huji.ac.il.

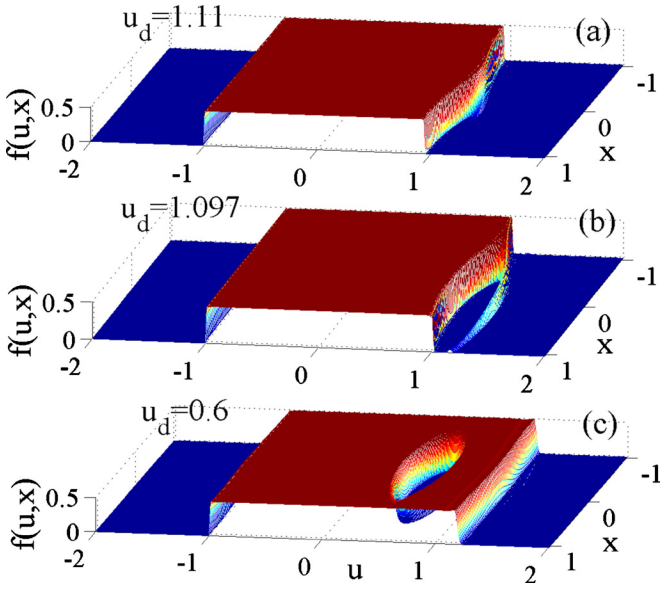

FIG. 1. (Color online) The formation of the autoresonant electron phase-space hole in the Vlasov–Poisson simulations in the chirped-down drive case: (a) a surface wave on the boundary of the phase-space fluid, (b) emergence of a void, and (c) a fully developed autoresonant hole.

large compared to the period of the driving perturbation. The averaged variational principle was developed by Whitham in the theory of slow modulations of nonlinear waves and comprises a nonlinear generalization of the WKB theory of linear waves. According to Whitham's approach, one averages the governing Lagrangian in a nonlinear wave propagation problem over the fast phase variable. Only slow dependent field variables remain in the averaged Lagrangian, which, upon variation with respect of these variables, yields slow evolution equations in the problem. The idea of using Whitham's principle in general autoresonant nonlinear wave interactions was proposed in Refs. 18 and 19 and illustrated in the problem of autoresonant excitation of large amplitude waves of the Sine–Gordon and Korteweg–de Vries equations. In the present work this approach is applied to chirped-driven, autoresonant BGK modes, the goal being a uniform description of all stages of excitation of these driven kinetic waves and addressing the modulational stability of the associated coherent phase-space structures.

The scope of the presentation will be as follows: In Sec. II we will present the results of our numerical Vlasov–Poisson simulations illustrating different regimes of excitation of kinetic autoresonant plasma waves. In Sec. III we will present our Eulerian, driven water bag model and the corresponding variational principle (to be used later in the Whitham's modulational theory). In the same section, we will apply our model in analyzing the initial phase-locking stage. This initial phase-locking is a necessary step for transition to fully developed autoresonance stage. In Sec. IV we will calculate the averaged Lagrangian in the problem and derive slow variational evolution equations describing autoresonant BGK modes. In the following Sec. V, we will focus on applications of the theory. In particular, we will consider formation of autoresonant waves for chirped-up or chirped-down driving frequency. In the same section, we will also present numerical simulations of autoresonant kinetic structures emerging via driving initially Maxwellian distributions by chirped frequency perturbations. Finally, Sec. VI will present our conclusions.

II. KINETIC AUTORESONANCE IN SIMULATIONS

Consider a one-dimensional (1D), *L*-periodic, *driven* Vlasov–Poisson's system[15]

$$f_t + uf_x - (E + E_d)f_u = 0, \quad E_x = 1 - \int f du, \tag{1}$$

where $f(x,u,t)$ $[f(x,u,t)=f(x+L,u,t)]$ is the electron velocity distribution in a plasma having a uniform initial electron density n_0, ions of the same density are assumed stationary, and $E(x,t)$ $[E(x,t)=E(x+L,t)]$ is the self-consistent electrostatic wave field. We also assume the presence of the external driving wave $E_d=\varepsilon \sin \theta_d$ (due to the ponderomotive effect of beating two transverse laser waves, for example) having amplitude ε, phase $\theta_d=kx-\int \omega_d(t)dt$, wave vector $k=2\pi/L$, and slowly *chirped* frequency $\omega_d(t)=\omega_0-\alpha t$, where α =const and either positive or negative for chirped-down or chirped-up driving frequency, respectively. We use dimensionless variables and parameters in Eq. (1), i.e., express u, x, and t in units of the characteristic (thermal) velocity u_{th} of the electrons, the Debye length $\lambda_D=u_{th}/\omega_p$, and the inverse plasma frequency ω_p, respectively. The distribution function is rescaled by n_0/u_{th} and the dimensionless fields are in units of $mu_{th}\omega_p/e$. We have solved our system numerically, using the same pseudospectral method[20] as in Ref. 15 for the case of spatially uniform flat-top initial distribution, $f\approx 1/2$ or 0 for $|u|<1$ or $|u|>1$, respectively. This distribution was modeled via $f(u,x,0)=C\exp(-u^{2n})\equiv f_0(u)$, where $n\gg 1$ $(n=250$ in simulations below), where $C\approx 1/2$ was the normalization constant. For avoiding numerical difficulties characteristic of Vlasov codes for distributions having large phase-space gradients, we have introduced artificial high frequency filters at grid scales in x and u. The accuracy of our code was tested by both comparing its results with those of the Lagrangian code[13] with and without the self-field and by varying the number of spectral harmonics. An important factor in the following examples is the location of the phase velocity of the free (undriven) plasma wave associated with our initial flat-top distribution. The linear theory yields dispersion relation $\omega_0^2=1+k^2$ for this wave and, therefore, its phase velocity $v_0=\sqrt{1+1/k^2}$ is outside the distribution, so the wave is Landau stable. Figures 1 and 2 show the results of our simulations for the case of the initial phase velocity $u_d(0)=\omega_d(0)/k$ of the driving wave above v_0 and slowly decreasing driving frequency. We used parameters $\varepsilon=0.01$, α $=0.003$, $k=3$, $u_d(0)=1.25$ (note that in this case $v_0\simeq 1.05$).

Figure 1 shows snapshots of the electron distribution in phase space as obtained in Vlasov–Poisson simulations at three stages of autoresonant excitation, i.e., the formation of a growing amplitude wavelike modulation of the plasma boundary [Fig. 1(a)], transition through the boundary [Fig. 1(b)], and fully developed phase-locked hole in phase space [Fig. 1(c)]. Note that the negative velocity boundary of the distribution is almost unaffected by the hole in Fig. 1(c), but

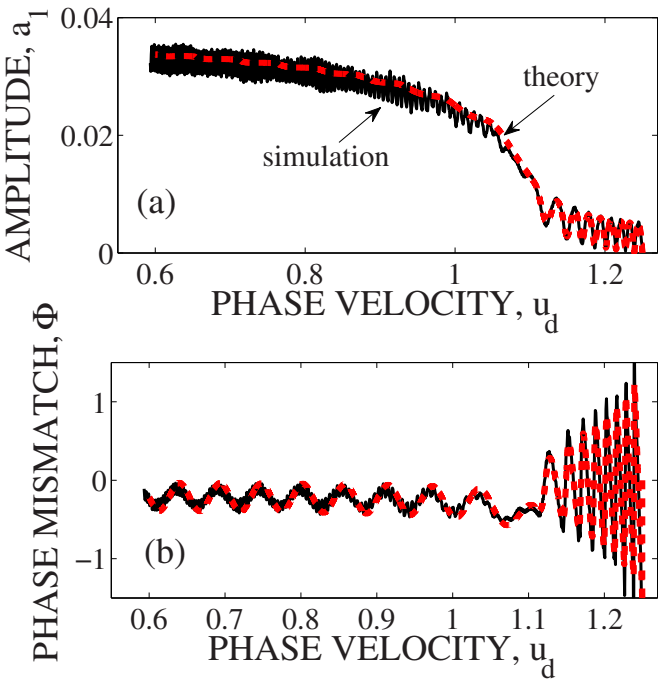

FIG. 2. (Color online) The evolution of an autoresonant BGK mode using chirped-down drive in the Vlasov–Poisson simulations (solid lines) and the theory (dashed lines). (a) The amplitude a_1 of the first self-field harmonic and (b) the phase mismatch of the driven BGK mode vs driving wave phase velocity.

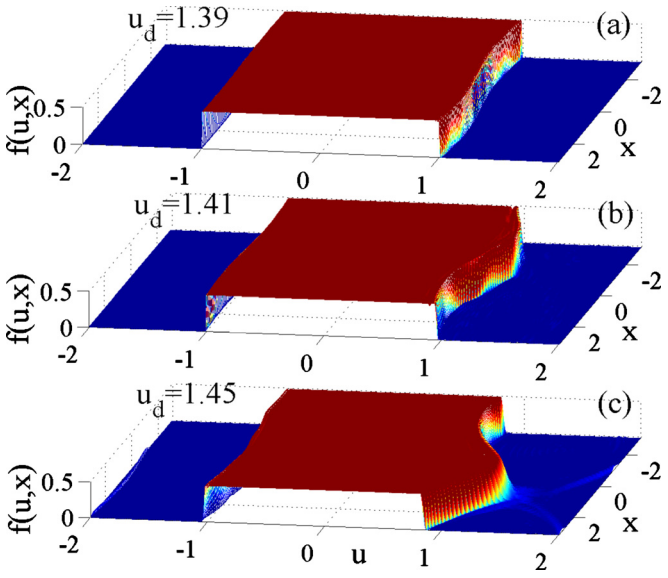

FIG. 3. (Color online) The formation of the autoresonant electron plasma wave in simulations in the chirped-up drive case: (a) the initial perturbation of the boundary of the phase-space fluid (u_d=1.39), (b) autoresonant wave at u_d=1.41, and (c) u_d=1.45.

the outer positive velocity boundary is displaced to higher velocities because of the conservation of the phase-space volume occupied by the distribution. This asymmetry in the distribution yields a dc current in the plasma,[15] which was analyzed recently in more detail in Ref. 21, as a possible new current drive mechanism. The evolution of the amplitude a_1 of the first spatial harmonic of the self-field and the phase mismatch Φ between the first harmonic and the driving wave in our example from Vlasov–Poisson are shown in Fig. 2 by solid lines, while the dashed lines represent our theory developed in Sec. IV. One observes the initial phase-locking process (at the driving wave phase velocity $u_d \gtrsim v_0$) in Fig. 2 at small excitation amplitudes, followed by autoresonant stage, where the phase mismatch Φ oscillates, but remains bounded, indicating a continuing phase-locking in the system as the driven wave traverses the region $u \lesssim v_0$ in phase space. Furthermore, in autoresonance, both the amplitude and the phase mismatch experience slow oscillating modulations reflecting the stability of the autoresonant excitation. When the driving phase velocity $u_d(t)$ is comparable to the ion acoustic speed, one may expect excitation of the acoustic waves. Nevertheless, this effect was neglected in the present work, assuming fast passage though the ion acoustic region, i.e., (dimensional) $\alpha \gg (k u_{th}^i)^2$, u_{th}^i being the ion thermal velocity.

A different autoresonant plasma wave excitation regime for the same initial distribution is illustrated in Figs. 3(a)–3(c), showing the snapshots of the distribution for the case when the initial $u_d(0)$ is still above the plasma distribution boundary at $u=1$, but below v_0. In this case, we *increase* the driving frequency and pass the resonance $u_d=v_0$ from below. We used parameters $\varepsilon=0.001$, $\alpha=-0.000\,02$, $k=1$, $u_d(0)=1.37$, while $v_0 \simeq 1.41$. The figure shows a growing amplitude modulation of the plasma boundary in phase space as the driving frequency increases. Because of the direction of the chirp, the gap between the driving phase velocity and the kinetic boundary of the plasma increases and we avoid the kinetic resonance, unless the modulation amplitude of the velocity boundary of the phase-space electron fluid becomes large to close the aforementioned gap. At these amplitudes we again observed formation of a phase-space hole, but it was numerically unstable in the example shown in Fig. 3. Additional data in the increasing driving frequency example are presented in Fig. 4, showing the evolution of the amplitude a_1 of the first spatial harmonic of the self-field and the phase mismatch Φ between the first harmonic and the driving wave. The solid lines in the figure represent our simulations, while the dashed lines correspond to the variational theory of Sec. IV. We observe that like Figs. 1 and 2 for the decreasing frequency drive, the initial phase-locking is established before the drive passes the $u_d=v_0$ resonance, while later the phase-locking continues as the amplitude of the excited plasma wave continues to grow in average. In addition, both the amplitude and the phase mismatch experience slow oscillating modulations indicating stability of the autoresonant solution.

Note that in both down- and up-driving frequency chirp cases (Figs. 1 and 2and Figs. 3 and 4, respectively), the excited plasma wave self-adjusts its parameters to stay in resonance with the drive continuously, despite the variation of parameters (driving frequency). This autoresonant phenomenon is well known in many other driven nonlinear systems.[22] For example, to adiabatically excite a pendulum to a large amplitude by an external oscillating perturbation, one needs to start at rest, sufficiently far from the linear resonance, and pass the resonance from above by slowly decreasing the driving frequency. In the small amplitude (lin-

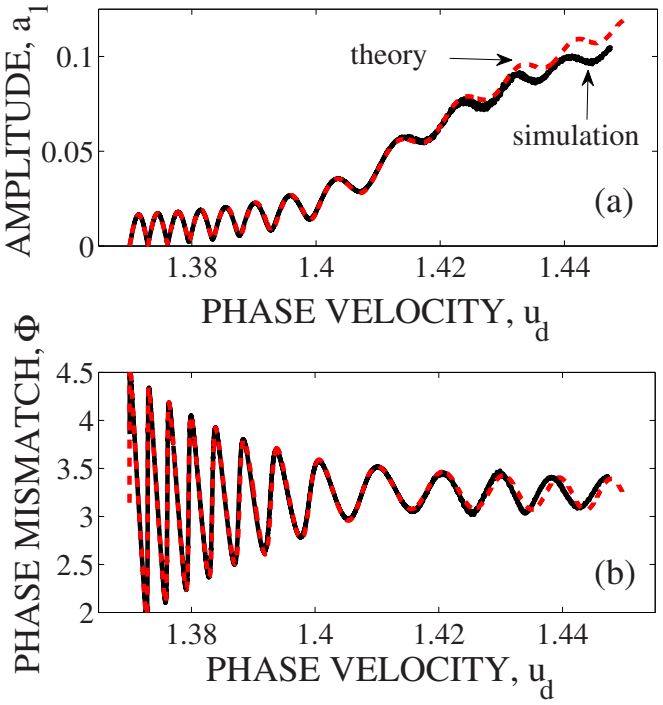

FIG. 4. (Color online) The evolution of autoresonant plasma wave using a chirped-up drive in simulations (solid lines) and theory (dashed lines). (a) The amplitude a_1 of the first self-field harmonic and (b) the phase mismatch of the driven BGK mode vs the phase velocity of the driving wave.

ear) excitation stage, chirped frequency driven pendulum and kinetic plasma waves are similar. In particular, the initial phase-locking in the driven system [see Figs. 2(b) and 4(b)] is established at this stage, prior to reaching the linear resonance. Since this is an important stage toward fully developed autoresonant evolution, we will discuss the linear excitation regime of autoresonant kinetic plasma waves in the next section, after presenting our Eulerian driven water bag model.

III. DRIVEN EULERIAN WATER BAG MODEL AND INITIAL PHASE-LOCKING STAGE

We adopt a 1D water bag model for describing evolution seen in Figs. 1 and 3, i.e., assume a uniform density electron phase-space distribution confined between well defined boundaries. The number of these boundaries in our problem is different before and after formation of the electron phase-space holes. Consequently, the sets of equations in our model at different excitation stages illustrated in Figs. 1 and 3 are different. Before the hole is formed, our system (dimensionless) describes the evolution of the driven electrostatic wave potential U and of the two boundaries $v_{1,2}(x,t)$ bounding the electron phase-space fluid

$$U_{xx} = \tfrac{1}{2}(v_1 - v_2) - 1, \tag{2}$$

$$v_{1,2t} + v_{1,2}v_{1,2x} = (U + U_d)_x, \tag{3}$$

where the driving potential, $U_d = \varepsilon' \cos\theta_d$ ($\varepsilon' = \varepsilon/k$), is periodic in x, but has chirped frequency $\omega_d(t) = \omega_0 - \alpha t$, as defined in Sec. II, and, initially, $U=0$, $v_{1,2} = \pm 1$. We introduce auxiliary potentials $\psi_{1,2}$, such that $v_{1,2} = (\psi_{1,2})_x$ and observe that Eqs. (2) and (3) can be derived from the variational principle $\delta \int L dx dt = 0$, where the three-field $(\psi_{1,2}, U)$ Lagrangian is

$$L = \frac{1}{2}(\psi_{1x} - \psi_{2x})(U + U_d) - U + \frac{1}{2}U_x^2 - \frac{1}{4}(\psi_{1x}\psi_{1t} - \psi_{2x}\psi_{2t}) - \frac{1}{12}(\psi_{1x}^3 - \psi_{2x}^3). \tag{4}$$

Similarly, after the formation of the phase-space hole, we follow the evolution of four boundaries $v_{1,2}$, $v_0^{\pm}$ ($v_0^{\pm}(x,t)$ being the upper and lower half-boundaries of the hole, respectively). The corresponding Eulerian system of equations is

$$U_{xx} = \tfrac{1}{2}[v_1 - v_2 - (v_0^+ - v_0^-)] - 1, \tag{5}$$

$$v_{1,2t} + v_{1,2}v_{1,2x} = (U + U_d)_x, \tag{6}$$

$$v_{0t}^{\pm} + v_0^{\pm}v_{0x}^{\pm} = (U + U_d)_x. \tag{7}$$

If, we define auxiliary potentials $v_{1,2} = (\psi_{1,2})_x$ and $v_0^{\pm} = (\psi_0^{\pm})_x$ for this case, Eqs. (5)–(7) can be derived from the variational principle with the five-field Lagrangian

$$L = \frac{1}{2}(\psi_{1x} - \psi_{2x} - \psi_{0x}^+ + \psi_{0x}^-)(U + U_d) - U + \frac{1}{2}U_x^2 - \frac{1}{4}(\psi_{1x}\psi_{1t} - \psi_{2x}\psi_{2t} - \psi_{0x}^+\psi_{0t}^+ + \psi_{0x}^-\psi_{0t}^-) - \frac{1}{12}(\psi_{1x}^3 - \psi_{2x}^3 - \psi_{0x}^{+3} + \psi_{0x}^{-3}). \tag{8}$$

The next goal is to use the variational formulations (4) and (8) of the problem and construct the Whitham's averaged variational principle for the system of interest. Our simulations suggest that the amplitude a_1 of the excited plasma wave and the phase mismatch Φ between the wave and the drive (see Figs. 2 and 4) comprise a set of slow variables in the fully developed autoresonant stage of excitation. We will use this set of variables in the next section describing the Whitham's approach to the problem. However, one also observes in Figs. 2 and 4 that zero initial conditions used in our simulations yield fast oscillations of both a_1 and Φ in the initial excitation stage (for $u \gtrsim 1.16$ in Fig. 2 and $u \lesssim 1.39$ in Fig. 4). Thus, one cannot use the Whitham's approach in the initial excitation stage until a_1 and Φ become sufficiently slow and the driven wave efficiently phase-locks to the drive. Fortunately, this initial nonadiabatic evolution occurs in a small amplitude (linear) evolution stage, which is discussed next.

In the initial phase-locking stage, we assume that the system proceeds from zero amplitude equilibrium $v_1 = 1$, $v_2 = -1$, $U=0$, and that the perturbations $\delta v_1 = v_1 - 1$, $\delta v_2 = v_2 + 1$ of the boundaries are sufficiently small for linearization of Eqs. (2) and (3)

$$U_{xx} = \tfrac{1}{2}(\delta v_1 - \delta v_2), \tag{9}$$

$$\delta v_{1t} + \delta v_{1x} = (U + U_d)_x, \tag{10}$$

$$\delta v_{2t} - \delta v_{2x} = (U + U_d)_x, \tag{11}$$

We seek periodic solutions of this system of form $U = Re[\tilde{U}(t)\exp(ikx)]$ and $\delta v_{1,2} = Re[\widetilde{v_{1,2}}(t)\exp(ikx)]$. By substituting these solutions into Eqs. (9)–(11), we obtain

$$-k^2\tilde{U}_t = \tfrac{1}{2}(\widetilde{\delta v_1} - \widetilde{\delta v_2}), \tag{12}$$

$$\widetilde{\delta v_{1t}} + ik\widetilde{\delta v_1} = ik(\tilde{U} + \tilde{U}_d), \tag{13}$$

$$\widetilde{\delta v_{2t}} - ik\widetilde{\delta v_2} = ik(\tilde{U} + \tilde{U}_d), \tag{14}$$

where $\tilde{U}_d(t) = (\varepsilon'/2)\exp[-i\int\omega_d(t)dt]$, as follows from the definition of U_d. The differentiation of the first equation in this system with time and the use of the last two equations yields a driven harmonic oscillator problem

$$\tilde{U}_{tt} + \omega_0^2\tilde{U} = -\tilde{U}_d, \tag{15}$$

where $\omega_0^2 = 1 + k^2$ was already defined in Sec. II. The solution of this chirped-driven problem can be written as a sum of a general solution of the free (undriven) problem and a particular solution of the driven oscillator

$$\tilde{U} = A\exp(-i\omega_0 t) + B(t)\exp\left[-i\int\omega_d(t)dt\right], \tag{16}$$

where A is a constant and the driven part is approximated by the adiabatically varying oscillation having the slowly varying frequency $\omega_d(t)$ of the drive. Here, in the adiabatic approximation, we assume $B_t \ll \omega_d B$, yielding $B(t) \approx \varepsilon'/2/[\omega_d(t)]^2 - \omega_0^2$. On the other hand, from the zero initial condition, we find $A = -\varepsilon'/2/[\omega_d(t=0)]^2 - \omega_0^2$. Initially, the two terms in Eq. (16) have equal amplitudes, but later, the amplitude of the driven mode $B(t)$ grows as the driving frequency approaches ω_0. Therefore, if starting sufficiently far from resonance, the driven part in the solution becomes dominant, explaining the initial phase-locking of the wave to the drive. At the same time, both the amplitude and the phase mismatch become slow, as the second term in Eq. (16) becomes dominant. We used the condition $B = 2A$ in our calculations for determining the time t_a of entering the adiabatic evolution stage (the corresponding values of the driving phase velocity were $u_d = 1.16$ in Fig. 2 and 1.39 in Fig. 4). At $t = t_a$, Eq. (16) yielded initial conditions for further evolution of the wave, as its amplitude continued to grow and the system approached the nonlinear evolution stage. Assuming that the adiabaticity of a_1 and Φ is continuously preserved beyond t_a, we switched to the description via Whitham's averaged variational principle, which is valid uniformly in both the linear and nonlinear stages of adiabatic evolution. This theory is presented next.

IV. AVERAGED VARIATIONAL PRINCIPLE FOR KINETIC AUTORESONANT PLASMA EXCITATIONS

A. Prehole formation stage

The main assumption of the Whitham's averaged variational approach is the separation of scales, such that the wave $U(x,t) = U(\theta)$ (in our case U is the electrostatic wave potential) is 2π-periodic in fast variable $\theta(x,t)$, but the associated frequency $\omega = -\partial\theta/\partial t$ and wave vector $k = \theta_x$ are slow (k = const in our problem). The theory below uses this assumption, but, in addition, assumes near phase-locking between the drive and the driven wave U, i.e., views the phase mismatch $\Phi = \theta_d - \theta$ as a slow object, assumed to be near 0 or π. Let $U(\theta)$ be an even function of θ and split the driving potential into the in- and out-of-phase components $U_d^0 = \varepsilon'\cos\theta\cos\Phi$ and $U_d^1 = -\varepsilon'\sin\theta\sin\Phi$ and rewrite the Lagrangian (4) in the form

$$L = L^0 + L^1, \tag{17}$$

where

$$L^0 = \frac{1}{2}(\psi_{1x} - \psi_{2x})(U + U_d^0) - U + \frac{1}{2}U_x^2 - \frac{1}{4}(\psi_{1x}\psi_{1t} - \psi_{2x}\psi_{2t}) - \frac{1}{12}(\psi_{1x}^3 - \psi_{2x}^3) \tag{18}$$

and

$$L^1 = \tfrac{1}{2}(\psi_{1x} - \psi_{2x})U_d^1. \tag{19}$$

Next, we seek solutions for $\psi_{1,2}$ in the form

$$\psi_{1,2} = \xi_{1,2} + V_{1,2}(\theta), \tag{20}$$

where $(\xi_{1,2})_t \equiv -\gamma_{1,2} = 0$, and $(\xi_{1,2})_x \equiv \beta_{1,2}$. Note that, since $(\beta_{1,2})_t + (\gamma_{1,2})_x = 0$, $\beta_{1,2}$ remain constant in time. We will also assume that similar to U, V is 2π-periodic and odd function in θ and that the average $\langle U\rangle$ over θ is zero. Note that $\beta_{1,2} = \langle v_{1,2}\rangle$ and we set initially for the unperturbed fluid, $\beta_{1,2} = v_{1,2} = \pm 1$. Now, we calculate the Whitham's averaged Lagrangian by fixing all slow dependent variables and parameters in Eq. (4) at some given time and averaging over θ between 0 and 2π. The averaged Lagrangian is $\bar{L} = \overline{L^0}$, since $\overline{L^1} = 0$. Prior to calculating $\overline{L^0}$, we substitute Eq. (20) into Eqs. (18) and (19), replace $(V_{1,2})_t$ by $-u_p(V_{1,2})_x$, where $u_p = \omega/k$ is the phase velocity of the driven wave, and consider the "*dynamical*" problem (in x) governed by Lagrangian (17) with all slow parameters fixed. Then, L^0 becomes

$$L^0 = \frac{1}{2}(V_{1x} - V_{2x})(U + U_d^0) + U_d^0 + \frac{1}{2}U_x^2 - \frac{1}{12}(V_{1x}^3 - V_{2x}^3) + \frac{1}{4}(u_p - 1)(V_{1x}^2 + V_{1x}) - \frac{1}{4}(u_p + 1)(V_{2x}^2 - V_{2x}). \tag{21}$$

Note that we omitted terms not containing the dependent fields in Eq. (21) as not contributing the dynamics. The three degrees of freedom problem (for U and $V_{1,2}$) with fixed parameters described by Eq. (21) is integrable. Indeed, we have two conserved canonical momenta $p_{1,2} = \partial L^0/\partial V_{1,2x}$, i.e.,

$$p_1 = -\tfrac{1}{4}V_{1x}^2 + \tfrac{1}{2}(u_p - 1)V_{1x} + \tfrac{1}{4}(u_p - 1) + \tfrac{1}{2}(U + U_d^0), \tag{22}$$

$$p_2 = \tfrac{1}{4}V_{2x}^2 - \tfrac{1}{2}(u_p + 1)V_{2x} + \tfrac{1}{4}(u_p + 1) - \tfrac{1}{2}(U + U_d^0). \tag{23}$$

These relations can be used to express V_{1x} and V_{2x} in terms of $U + U_d^0$

$$V_{1x} = u_p - 1 - s_1, \tag{24}$$

$$V_{2x} = u_p + 1 - s_2, \tag{25}$$

where, instead of $p_{1,2}$, we used different conserved variables $B_1 = -2p_1 + (u_p/2)(u_p - 1)$, $B_2 = 2p_1 + (u_p/2)(u_p + 1)$ and defined

$$s_{1,2} = [2(B_{1,2} + U + U_d^0)]^{1/2}. \tag{26}$$

In addition to $B_{1,2}$, the "energy function"

$$A = U_x^2 + p_1 V_{1x} + p_2 V_{2x} - L^0 \tag{27}$$

is also conserved in the fixed parameters case. The reduction to the integrable one degree-of-freedom problem is completed by substituting Eqs. (24), (25), and (21) in Eq. (27). This yields the standard "energy" conservation law for variable U involving an effective potential

$$\tfrac{1}{2}U_x^2 + V_{\text{eff}} = A', \tag{28}$$

where

$$V_{\text{eff}} = -\tfrac{1}{2}u_p^2 - \tfrac{1}{2}(u_p - 1)B_1 + \tfrac{1}{2}(u_p + 1)B_2 + \tfrac{1}{6}(s_1^3 - s_2^3) + (U + U_d^0) \tag{29}$$

and $A'_{1,2} = A + 1/6$. By averaging in Eq. (27) over θ, we obtain

$$\bar{L} = \overline{L^0}(A', B_1, B_2; \omega, k, \Phi) = \langle U_x^2 \rangle - A' = kI(A', B_1, B_2; \omega, k, \Phi) - A', \tag{30}$$

where

$$I = \frac{1}{2\pi k}\int_0^{2\pi} U_x^2 d\theta = \frac{1}{2\pi}\oint [2(A' - V_{\text{eff}})]^{1/2} dU \tag{31}$$

is the usual canonical action governed by Eq. (21). Finally, four slow evolution equations in the problem are obtained from $\bar{L}$ by taking variations with respect to A, $B_{1,2}$, and θ (recall that $\omega = -\theta_t$, $k = \theta_x$ and $\Phi = \theta^d - \theta$).

At this stage, to further simplify our problem, we will depart from the general procedure outlined above. The idea is based on the assumption of near-harmonicity (still preserving the nonlinearity in the problem) of U, i.e., we set $U \approx a_1' \cos\theta + a_2' \cos 2\theta$ (where $a_i' = a_i/k$), ignore higher harmonics, and view the amplitudes $a_{1,2}$ as new slow dependent variables. This approach gave a very good agreement with numerical simulations of the driven electron holes in Ref. 16 using the ideal phase-locking approximation, so the same approach is used in the averaged variational principle. To this end, we average in Eq. (28), to get

$$A' = \tfrac{1}{2}\langle U_x^2 \rangle - \tfrac{1}{2}u_p^2 - \tfrac{1}{2}(u_p - 1)B_1 + \tfrac{1}{2}(u_p + 1)B_2 + \tfrac{1}{6}(\langle s_1^3 \rangle - \langle s_2^3 \rangle), \tag{32}$$

which, after substitution in Eq. (27) and using $\langle U_x^2 \rangle = \frac{1}{2}a_1^2 + 2a_2^2$, yields

$$\bar{L} = \tfrac{1}{4}a_1^2 + a_2^2 + \tfrac{1}{2}u_p^2 + \tfrac{1}{2}(u_p - 1)B_1 - \tfrac{1}{2}(u_p + 1)B_2 - \tfrac{1}{6}(\langle s_1^3 \rangle - \langle s_2^3 \rangle), \tag{33}$$

where

$$\langle s_{1,2}^3 \rangle = \frac{1}{2\pi}\int_0^{2\pi} \{2[B_{1,2} + (a_1' + \varepsilon' \cos\Phi)\cos\theta + a_2' \cos 2\theta]\}^{3/2} d\theta. \tag{34}$$

Our averaged Lagrangian in this approximation becomes a function of slow variables $\bar{L} = \bar{L}(a_1, a_2, B_1, B_2; \omega, k, \Phi)$. By taking variations with respect to $a_{1,2}$, $B_{1,2}$, and θ, we obtain the desired slow evolution system. For example, by varying with respect to $a_{1,2}$ we have

$$ka_1 = \langle (s_1 - s_2)\cos\theta \rangle \tag{35}$$

and

$$4ka_2 = \langle (s_1 - s_2)\cos 2\theta \rangle. \tag{36}$$

The variations with respect to $B_{1,2}$ yield two additional algebraic equations

$$\langle s_1 \rangle = u_p - 1, \quad \langle s_2 \rangle = u_p + 1 \tag{37}$$

while the variation with respect to θ results in

$$(B_1 - B_2 + 2u_p)_t = \varepsilon \langle (s_1 - s_2)\cos\theta \rangle \sin\Phi. \tag{38}$$

Note that by setting $\Phi = 0$, $\omega = \omega_d(t)$, and $a_2 = 0$, Eqs. (35)–(37) yield the system used in our ideal phase-locking approximation Ref. 16. Indeed, with this substitutions, Eq. (35) is the dispersion relation in our previous theory, while Eq. (37) is the old action conservation law. Now, with the new variational formulation, the phase mismatch Φ becomes an additional slow dependent variable and a new variational Eq. (38) makes the set of equations for a_1, a_2, B_1, B_2, and Φ complete, removing $\Phi = 0$ assumption of the old theory. In our numerical examples above we have solved Eqs. (35)–(38) numerically by differentiating the algebraic Eqs. (35)–(37) with respect to time, thus converting the problem into a set of first order differential equations for $a_{1,2}$, $B_{1,2}$, and Φ. The solutions of this set (dashed lines in Fig. 2 for $1.1 \lesssim u_d \lesssim 1.16$ and in Fig. 4 for $1.39 \lesssim u_d$) are in an very good agreement with Vlasov–Poisson simulations, but the theory can be used prior to formation of the phase-space hole only. Furthermore, we have found that for chirped down case, yielding the hole formation, the inclusion of the second harmonic did not changed the evolution significantly. In contrast, in the chirped up case (see Sec. V A) the inclusion of the second harmonic was essential because of significantly higher amplitudes of excitations, but in this case the formation of the phase-space hole did not take place until very large excitation amplitudes. In principle, in this case we could include higher harmonics in the theory, but this extension was outside the scope of the present work. Returning to the down-chirped case, the hole formation takes place as u^d decreases and the energy B_1 of the limiting trajectory v_1 approaches $a_1' + \varepsilon' \cos\Phi$, i.e., v_1 approaches the separatrix at some time $t = t_*$. One can estimate the value of u_d at this stage as $u_d^* = 1 + 8/\pi(a_1^{*\prime} + \varepsilon_1' \cos\Phi^*)^{1/2}$. In the example in Fig. 2 u_d^* was equal to 1.1. At the moment of hole formation, some of the phase fluid flows around the separatrix [see simulations in Fig. 1(b)] and reconnects with the rest of the fluid due to a small dissipation, introduced in the simulations (for dealing with the singularities of the Vlasov code at sharp phase-

space boundaries). After the reconnection, the electron phase-space hole is formed, having nearly the form of the separatrix. Our adiabatic analysis fails near the separatrix because of the large period of the trajectory. However, if the variation of u_d is sufficiently slow, one can approach a close vicinity of the separatrix without breaking the adiabatic invariance. After the hole is formed, its boundary yields an additional limiting trajectory in the bulk of the distribution (see similar developments in Ref. 16 assuming ideal phase-locking in the system). This requires modification of the theory, which is described next.

B. Inclusion of a phase-space hole in the theory

Since the hole boundaries comprise a doubly valued function of velocities, we view the hole as confined between two single valued functions of velocity. The derivation of the averaged Lagrangian in this case is similar to that described above, yielding (see Appendix)

$$\bar{L} = \frac{1}{4}a_1^2 - \frac{1}{4}u_p^2(-\beta_1 + \beta_2 + \beta_0^+ - \beta_0^-) - \frac{u_p}{4}(\beta_1^2 - \beta_2^2 - \beta_0^{+2} + \beta_0^{-2}) + \frac{1}{2}(u_p - \beta_1)B_1 - \frac{1}{2}(u_p - \beta_2)B_2 - \frac{1}{2}(u_p - \beta_0^+)B_0^+ + \frac{1}{2}(u_p - \beta_0^-)B_0^- + \frac{1}{6}(\langle s_1^3\rangle + \langle s_2^3\rangle - \langle s_0^{+3}\rangle - \langle s_0^{-3}\rangle) - \frac{1}{4}\langle \beta_0^+\gamma_0^+ - \beta_0^-\gamma_0^-\rangle, \tag{39}$$

where now we have defined $\psi_0^\pm = \xi_0^\pm + V_0^\pm(\theta)$, $(\xi_0^\pm)_t = -\gamma_0^\pm$ (superscripts $\pm$ corresponding to the upper and lower hole boundaries) and assumed that $V_0^\pm$ is again 2π-periodic in θ, while $\beta_0^\pm = \langle v_0^\pm\rangle$. In addition, we defined $B_0^+ = 2p_0^+ + (u_p/2)\times(u_p - \beta_0^+) + \gamma_0^+/2$, $B_0^- = 2p_0^- + (u_p/k)(u_p - \beta_0^-) + \gamma_0^-/2$, where $p_0^\pm = \partial L/\partial V_{0x}^\pm$. We have also ignored the second spatial harmonic a_2 of the wave when the hole is present (the validity of this simplification in the down-chirped case was also verified via Vlasov–Poisson simulations), yielding

$$\langle s_{1,2}^3\rangle = \frac{1}{2\pi}\int_0^{2\pi}\{2[B_{1,2} + (a_1' + \varepsilon'\cos\Phi)\cos\theta]\}^{3/2}d\theta \tag{40}$$

and

$$\langle s_0^{\pm 3}\rangle = \frac{1}{2\pi}\int_0^{\theta_0^\pm}\{2[B_0^\pm + (a_1' + \varepsilon'\cos\Phi)\cos\theta]\}^{3/2}d\theta, \tag{41}$$

where $\theta_0^\pm = \arccos[-B_0^\pm/a_1' + \varepsilon'\cos\Phi]$.

Our averaged Lagrangian now becomes $\bar{L} = \bar{L}(a_1, B_1, B_2, B_0^\pm; \omega, k, \Phi)$. By taking variations with respect to a_1, $B_{1,2}$, $B_0^\pm$, and θ we obtain the desired slow evolution system. For example, variation with respect to a_1 gives

$$ka_1 = \langle(-s_1 - s_2 + s_0^+ + s_0^-)\cos\theta\rangle. \tag{42}$$

The variations with respect to $B_{1,2}$ and $B_0^\pm$ yield four additional algebraic equations

$$\langle s_1\rangle = \beta_1 - u_p,\ \langle s_2\rangle = u_p - \beta_2 \tag{43}$$

and

$$\langle s_0^+\rangle = \beta_0^+ - u_p,\ \langle s_0^-\rangle = u_p - \beta_0^-. \tag{44}$$

Finally, the variation with respect to θ results in

$$\left[\Delta B + u_p\Delta\beta + \tfrac{1}{2}(\beta_0^{+2} - \beta_0^{-2})\right]_t = \varepsilon\langle\Delta s\cos\theta\rangle\sin\Phi. \tag{45}$$

where $\Delta B \equiv B_1 - B_2 - B_0^+ + B_0^-$, $\Delta\beta \equiv \beta_1 - \beta_2 - \beta_0^+ + \beta_0^-$, and $\Delta s \equiv -s_1 - s_2 + s_0^+ + s_0^-$. Now, we assume that the "energies" $B_0^\pm$ of the two trajectories bounding the hole, are equal, i.e., $B_0^+ = B_0^- \equiv B_0$, $s_0^+ = s_0^- \equiv s_0$, and define $\Delta v = \langle v_1\rangle - 1$ (note that $(2\pi/k)\Delta v$ is the area of the hole). Then, one can show that

$$\Delta v = \frac{8}{\pi}\sqrt{a_1'^* + \varepsilon'\cos\Phi^*}, \tag{46}$$

where $a_1'^*$ and Φ^* are the values of a_1' and Φ at the moment of formation of the hole. Furthermore

$$\beta_1 = 1 + \Delta v,\ \ \beta_2 = -1 \tag{47}$$

while

$$\beta_0^\pm = u_p \pm \tfrac{1}{2}\Delta v. \tag{48}$$

Then, the desired set of slow variational equations becomes

$$ka_1 = \langle(-s_1 - s_2 + 2s_0)\cos\theta\rangle, \tag{49}$$

$$\langle s_1\rangle = 1 + \Delta v - u_p,\ \langle s_2\rangle = u_p + 1,\ \langle s_0\rangle = \frac{\Delta v}{2}, \tag{50}$$

$$(B_1 - B_2 + 2u_p)_t = \varepsilon\langle(-s_1 - s_2 + 2s_0)\cos\theta\rangle\sin(\Phi), \tag{51}$$

where we have neglected an additional term $u_p\Delta v$ in the square brackets in the left hand side of the last equation, assuming that the width of the hole is small compared to the width of the distribution in velocity space. As in Sec. IV A, setting $\Phi = 0$ and $\omega = \omega_d(t)$, in Eqs. (49) and (50) yields the system derived via the ideal phase-locking approximation in Ref. 16. Within the new variational formulation, Φ becomes a new dependent slow variable and the system of equations for a_1, $B_{1,2}$, and Φ is closed via Eq. (51), removing the limitations of the old theory when the hole is inside the bulk of the distribution. We have solved the system of slow Eqs. (49)–(51) numerically in the example in Fig. 2. The solution (dashed lines in Fig. 2 for $u_d \lesssim 1.1$) is again in a very good agreement with Vlasov–Poisson simulations and illustrates the continuous phase-locking of the excited BGK mode to the drive. The slow oscillating modulations around the averaged autoresonant solution manifest the intrinsic stability of autoresonance in the system, as the excited wave automatically adjusts its amplitude to stay in a continuous resonance with the drive. These modulations are characteristic of all autoresonant systems, while the robust stability makes excitation and control of autoresonant waves insensitive to the exact form of the driving frequency chirp as long as the chirp rate is sufficiently small.[22] In the next section we will discuss different autoresonance regimes in our system, present addi-

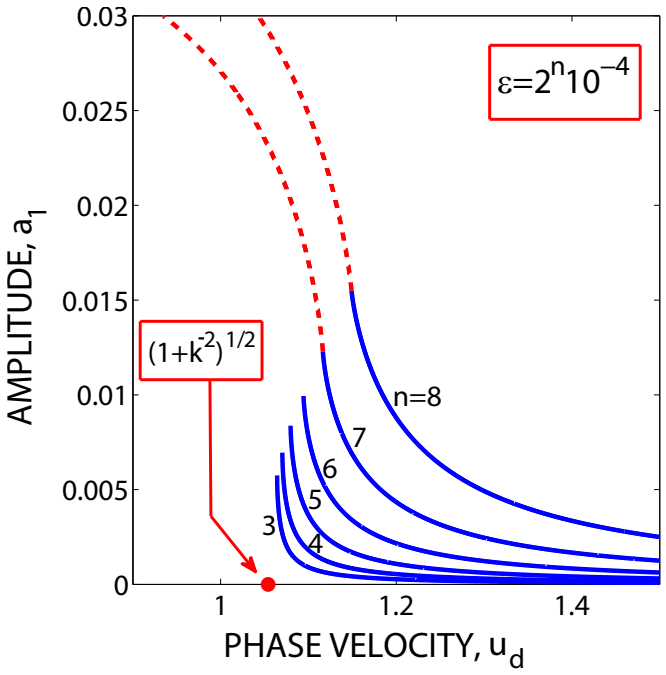

FIG. 5. (Color online) The amplitude a_1 of the driven BGK mode vs the driving wave phase velocity $u_d(t)$ using chirped-down drive with different driving amplitudes $\varepsilon=2^n10^{-4}$, $n=3,\ldots,8$, as given by the ideal phase-locking approximation before (black solid lines) and after (red dashed lines) the formation of a hole. Stable phase-space holes are formed for sufficiently large driving amplitudes only.

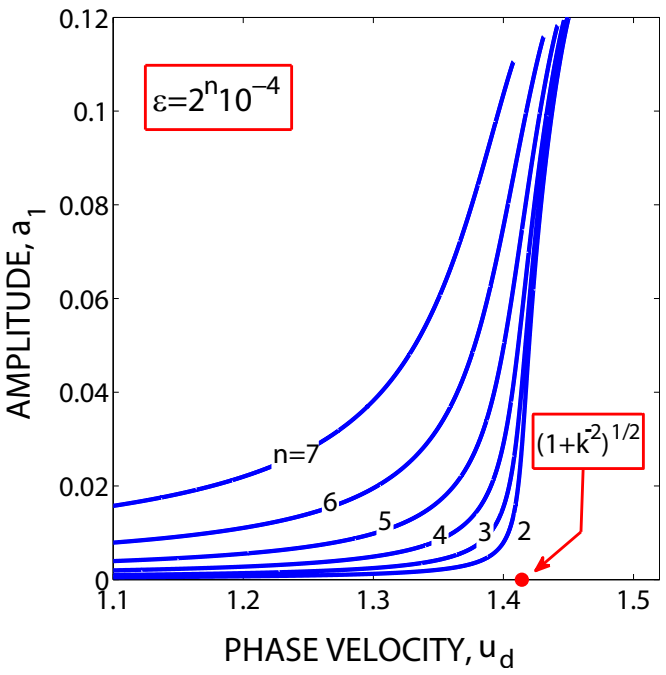

FIG. 6. (Color online) The amplitude a_1 of the driven plasma wave for different driving amplitudes $\varepsilon=2^n10^{-4}$, $n=2,3,\ldots,7$, as given by the ideal phase-locking approximation (solid lines).

tional examples of application of our variational theory, as well as simulations of autoresonant evolution for initially Maxwellian velocity distributions.

V. DISCUSSION AND FURTHER EXAMPLES

A. Passage through resonance in different directions

We have used our Lagrangian model in different scenarios of formation of kinetic autoresonant plasma waves and compared the predictions of our theory with simulations. One of such prediction is the possibility of excitation of autoresonant waves with both down- and up-chirped driving waves. The qualitative difference between the two processes can be illustrated by using the simplest ideal phase-locking (zero phase mismatch) assumption. The down-chirped autoresonance within this approximation was studied in Ref. 16. For illustration, Fig. 5 shows the amplitude a_1 of the first harmonic of the self-field versus the driving wave phase velocity $u_d(t)$ for a down-chirped drive having different driving amplitudes $\varepsilon=2^n10^{-4}$, $n=2,3,\ldots,8$, and $k=3$, before (black solid lines) and after (red dashed lines) the hole formation. One observes a threshold on the driving amplitude, such that $\varepsilon\gtrsim 0.01$ only leads to the hole formation. For lower ε, the excited field amplitude reaches the point, where its derivative with respect to $u_d(t)$ becomes infinite, destroying the adiabaticity of the process and the phase-locking in the system. Note that the passage trough the linear resonance v_0 ($v_0=1.054$ for the example in the figure) is necessary for formation of the autoresonant hole in phase space. If one starts with the drive below v_0 and down-chirps its frequency, the autoresonance does not develop. On the other hand, if one proceeds from below v_0, but chirps the driving frequency up, the autoresonant excitation in the system may take place. For example, Fig. 6 shows a_1 versus $u_d(t)$ using the up-chirped drive with different driving amplitudes $\varepsilon=2^n10^{-4}, n=2,3,\ldots,7$, and $k=1$, as given by the theory from Ref. 16. In this case, the passage through v_0 ($v_0=1.41$ for the example in the figure) ensures a significant autoresonant growth of the self-field amplitude, but does not lead to formation of a stable phase-space hole. A similar behavior is found in Vlasov–Poisson simulations and described via the full averaged Lagrangian theory, as illustrated in Figs. 1–4 for both up- and down-chirped drives.

The use of chirped frequency driving waves allows to control autoresonant BGK modes by using more complex schemes of variation of driving parameters than illustrated in previous examples. The control is stable and robust as long as the variation of the driving parameters is sufficiently slow. We illustrate this robustness in both simulations and the variational theory in Figs. 7 and 8 showing the same example as in Figs. 1 and 2, but first saturate the decrease of the driving frequency adiabatically at $u_d=0.8$ and then slowly decrease the driving amplitude ε to 10% of its initial value ($\varepsilon=0.01$). The self-field amplitude a_1 and the phase mismatch Φ in this example are shown in Figs. 8(a) and 8(b), respectively. The full lines in the figure represent the results of the simulations, the theory is shown by dashed lines, while the snapshots of the electron distributions in phase space in simulations at three different times are shown in Fig. 7. One can see that the phase-space hole remains stable despite the reduction of the driving amplitude ε, but after the reduction, the hole becomes elongated in x and narrower in u, preserving its area, which is an adiabatic invariant. This

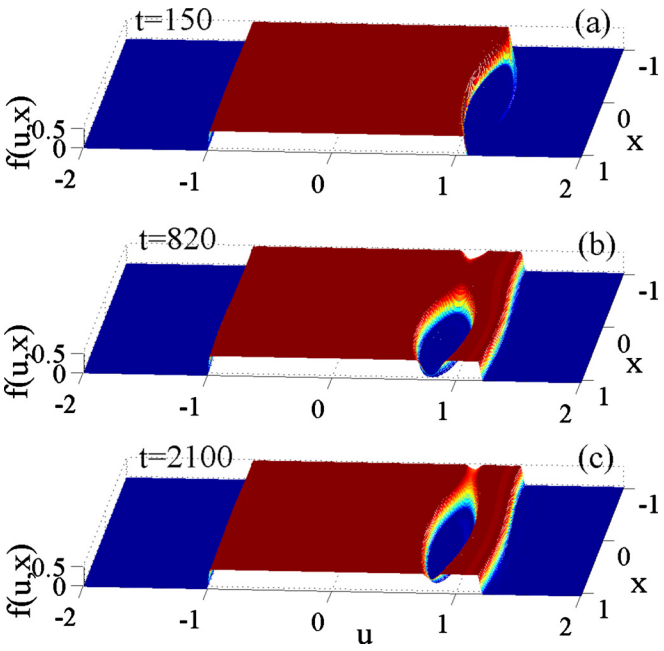

FIG. 7. (Color online) The control of an electron phase-space hole by driving parameters in simulations: (a) emergence of the hole via constant driving frequency chirp rate, (b) a stable phase-space hole after the down-chirp rate saturates, and (c) nearly free stable phase-space hole (the driving amplitude is decreased adiabatically to one tenth of its original value.

deformation of the hole yields only a 25% decrease of the self-field amplitude. We also observe a very good agreement of simulations with the predictions of the averaged Lagrangian theory.

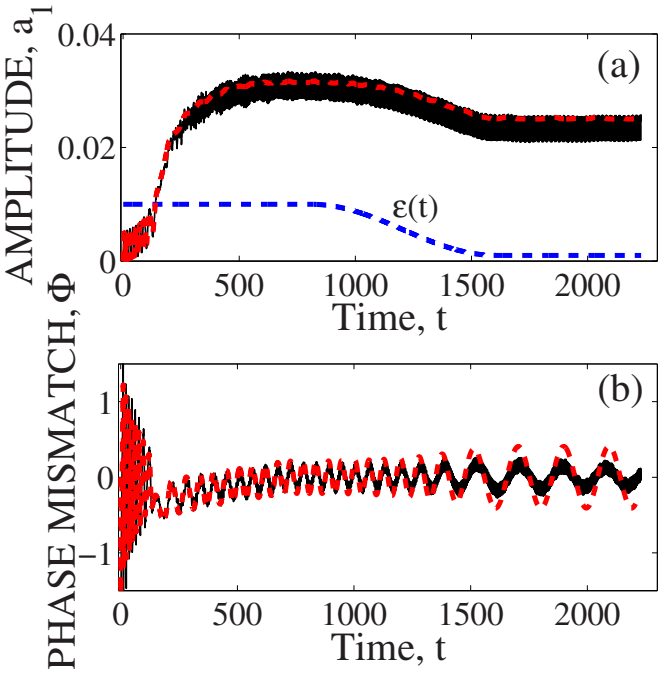

FIG. 8. (Color online) The evolution of autoresonant BGK mode in the case when the driving parameters ω_d and ε are changed adiabatically; simulations (black solid lines) and theory (red dashed lines). (a) The amplitude a_1 of the first self-field harmonic and (b) the phase mismatch of the driven BGK mode vs time.

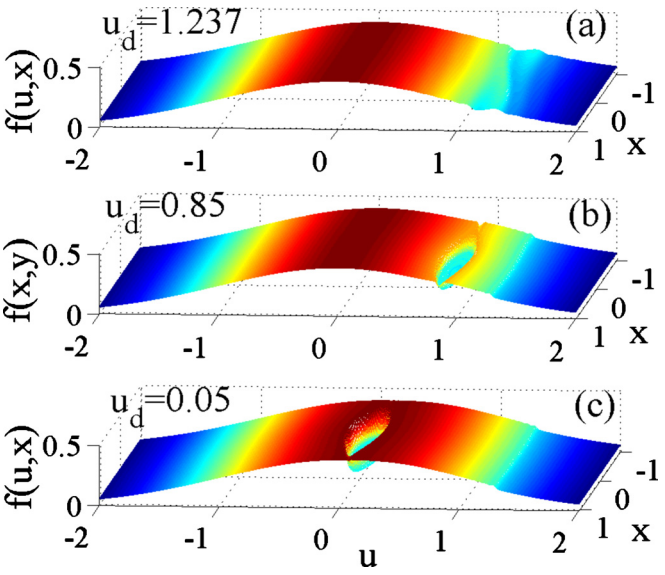

FIG. 9. (Color online) The driven phase-space depression formed by a chirped frequency driving wave in a Maxwellian distribution. The structures are shown at three different evolution times, as the driving wave phase velocity assumes the values (a) $u_d=1.237$, (b) $u_d=0.85$, and (c) $u_d=0.05$.

B. Autoresonant kinetic waves for Maxwellian distributions

Coherent electron phase-space structures similar to those discussed above can be formed in a plasma by a chirped frequency drive when starting from more realistic, smooth initial phase-space distributions. Previously, formation of phase-space holes in such cases was studied via a multiwater bag model within the ideal phase-locking assumption.[16] Here, we discuss formation of autoresonant coherent structures for initially Maxwellian distributions in simulations. Figure 9 shows snapshots of the electron distribution function in the down-chirped case obtained using our Vlasov–Poisson solver, while starting with distribution $f=(2\pi)^{-1/2}\exp(-u^2/2)$ and using driving parameters $k=3$, $\alpha=0.003$, and $\varepsilon=0.01$. The figure illustrates formation and evolution of a growing depression in the electron phase-space distribution with the local minimum drifting in velocity space toward the center of the distribution, as the driving frequency decreases and assumes values 1.237, 0.85, and 0.05 at three different times. Note that the initial driving wave phase velocity $[u_d(0)=1.25]$ in our simulations was significantly smaller than the linear plasma wave phase velocity $v_0=\sqrt{3+1/k^2}=1.76$ in this example. Additional data from the simulations are presented in Fig. 10, showing the evolution of a_1 and Φ versus down-chirped driving phase velocity. One again observes the growing self-field in the wave and the continuing phase-locking with the drive, as the hole traverses the distribution in phase space. Nonetheless, because of the finite chirp rate α, the phase mismatch settles at $\Phi\approx 0.25$. This value cannot be obtained within the ideal $(\Phi=0)$ phase mismatch theory.[16] In principle, one can still use the multiwater bag model and develop the corresponding averaged variational principle. However, because of the ex-

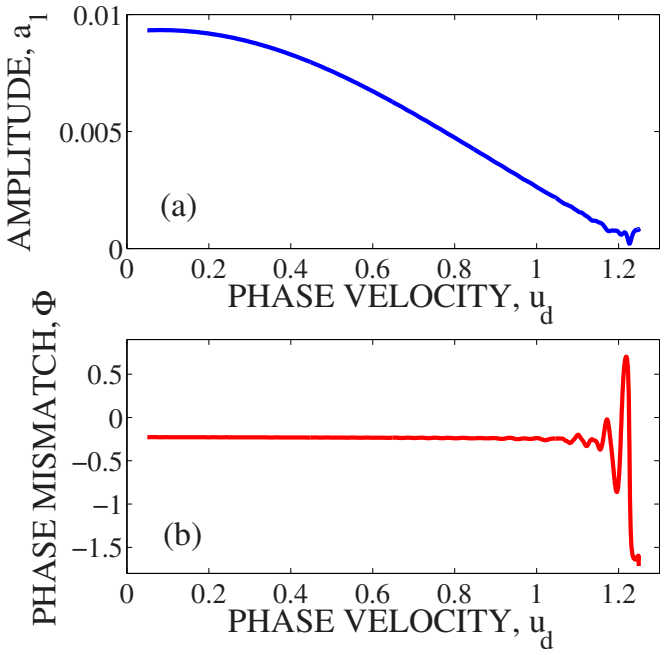

FIG. 10. (Color online) The evolution of the autoresonant BGK mode excited via down-chirped drive for Maxwellian initial distribution. (a) The amplitude a_1 of the first self-field harmonic and (b) the phase mismatch of the driven BGK mode vs phase velocity.

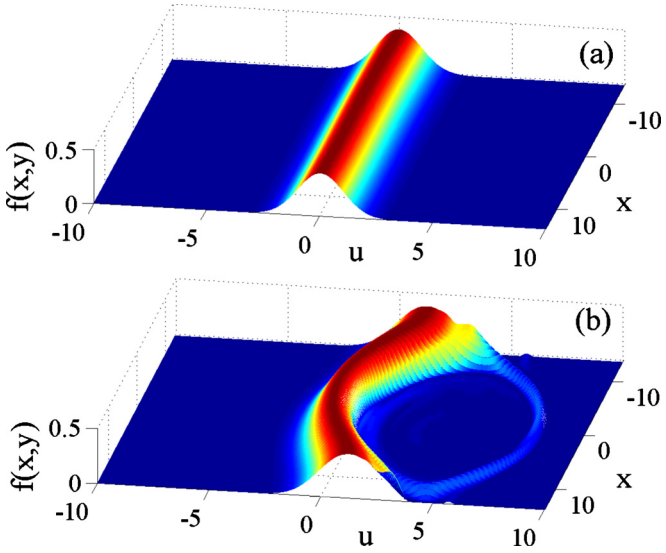

FIG. 11. (Color online) Large amplitude phase-space excitation formed by a chirped-up frequency drive in the case of initially Maxwellian distribution. The waves are shown (a) at the beginning (u_d=3) of the excitation process and (b) just before the autoresonance is lost (u_d=4.13).

pected significant increase of the independent variables in this problem, such a development remained outside the scope of the present work.

Next, we show the results of simulations for the same initial Maxwellian distribution, but chirping the drive frequency up (for driving parameters k=0.277, α=−0.001, and ε=0.05). In this case, the linear resonance corresponds to v_0=4. We have started the simulations with the initial driving phase velocity $u_d(0)$=3, i.e., below the linear resonance and with only a negligible fraction of the electrons in the kinetic resonance with the drive. The passage through resonance in this case yielded formation of a very large deformation of the phase-space distribution seen in Fig. 11. This effect is due to nearly two orders of magnitude larger self-field amplitudes excited with the chirped-up frequency drive (see the results for a_1 and Φ in Fig. 12) before the phase-locking is lost, as compared to those for chirped-down drives.

The last interesting phenomenon discussed below is the formation and control of an autoresonant clump in phase space. The effect is seen if one repeats the previous simulation, but applies the drive with a phase velocity resonating with a larger fraction of the distribution initially [$u_d(0)$=1.8 in the simulations below]. We used parameters k=1, α=−0.000 05, and ε=0.02, so that v_0=2. As the driving frequency increases, particles having velocities close to the driving velocity initially are trapped in Cherenkov resonance and are displaced (accelerated) to higher velocities, forming a bump in phase space, as shown in Fig. 13. Figure 14 shows the corresponding evolution of a_1 and Φ in this case. Again, one observes that the self-field grows as the phase-locking with the drive continues. However, in contrast to other kinetic structures discussed in the paper, the spatially localized clump in phase space shown in Fig. 13 is only stable if the driving field is present and the localization is destroyed if the drive is turned off.

VI. CONCLUSIONS

In conclusion:

(a) We have studied 1D evolution of initially flat-top electron phase-space distribution driven by an external, ponderomotive, chirped frequency wave passing

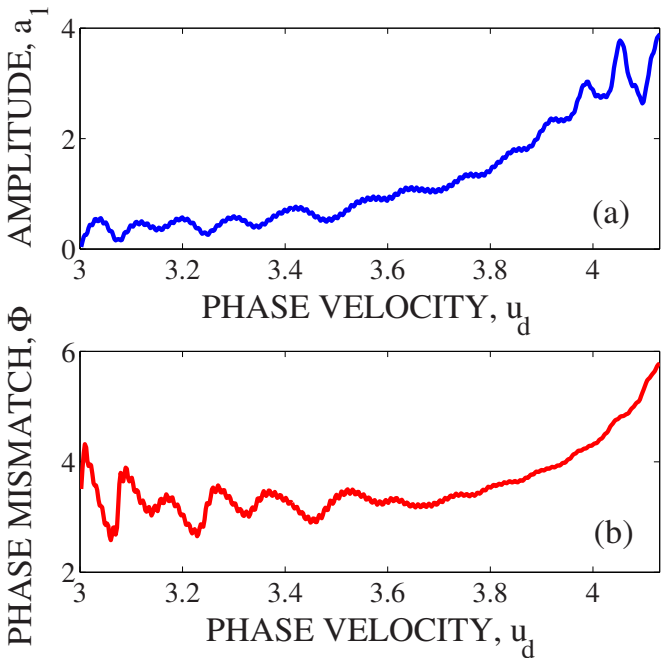

FIG. 12. (Color online) The evolution of the autoresonant BGK mode excited by a chirped-up drive for Maxwellian initial distribution. (a) The amplitude a_1 of the first self-field harmonic and (b) the phase mismatch of the driven BGK mode vs driving phase velocity.

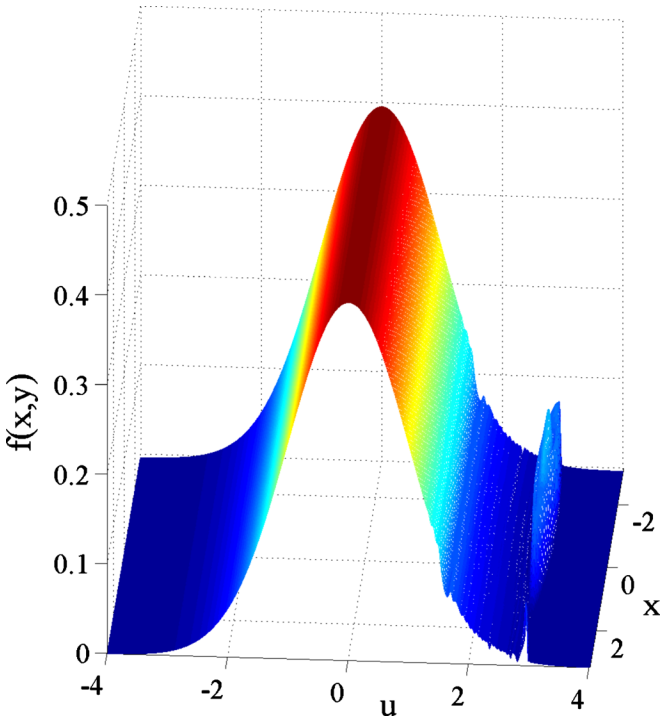

FIG. 13. (Color online) The driven phase-space clump formed by an up-chirped frequency driving wave in an initially Maxwellian distribution. The clump is shown at time, when the driving wave phase velocity is u_d=2.85.

through resonances in the problem. Numerical simulations show existence of different scenarios of formation of autoresonant (continuously phase-locked) kinetic structures in this system for sufficiently slow chirp rate of the driving frequency. In some cases, the distribution forms electron holes in phase space, while the electric field associated with these holes comprises a slowly evolving, driven BGK mode.

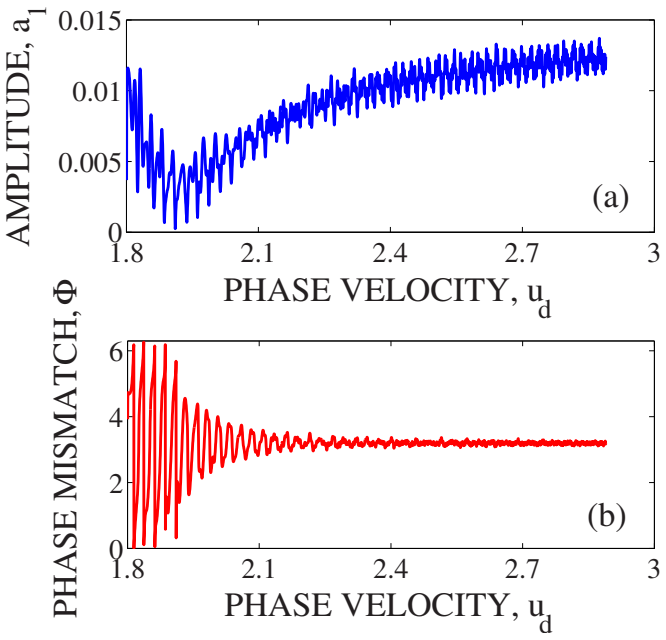

FIG. 14. (Color online) The evolution of the autoresonant BGK mode associated with a clump in phase space excited by a chirped-up drive for Maxwellian initial velocity distribution. (a) The amplitude a_1 of the first self-field harmonic and (b) the phase mismatch of the driven wave vs the driving phase velocity.

(b) An averaged Lagrangian (Whitham's) approach, based on the water bag model, was developed for analyzing autoresonant excitations in the system. The theory uses Eulerian description of the boundaries (limiting trajectories) confining a flat electron distribution in phase space. The associated Lagrangian is averaged over the fast time scale associated with the driving frequency, yielding the averaged Lagrangian for the slow variables in the problem, including the effective energies B_i of the limiting trajectories, the amplitudes a of the driven electrostatic wave, and its phase mismatch Φ with the drive. The variations with respect to these variables lead to a set of algebraic and ordinary differential equations describing the autoresonant evolution of the driven system. The addition of the dynamics of Φ in the problem makes the theory complete, as compared to the approach based on a perfect phase-locking (Φ =0) assumption of Ref. 16. Generally, we have seen a very good agreement between the predictions of our Lagrangian theory and simulations.

(c) The averaged variational formulation reduces our driven problem to the solution of a set of algebraic and ordinary differential equations. The number of variational evolution equations in the problem depends on the number of the limiting trajectories describing the evolution of the distribution in phase space. This number varies from 4 (or 5 if the second harmonics of the field is included), see Eqs. (35)–(38), to 5 (or 6) when the electron phase-space hole is formed; see Eqs. (49)–(51). In principle, the case of an arbitrary initial distribution can be treated similarly within a multiwater bag model, where one views the initial distribution as a set of superimposed thin flat-top distributions (layers). The number of evolution equations in this case will increase in proportion to the number of layers in the initial distribution.

(d) Formation of autoresonant kinetic structures described above requires passage through the linear resonance in the problem. We used our Eulerian water bag model to show that the driven wave is efficiently phase-locked to the drive prior passage through the linear resonance, provided the drive starts sufficiently far from the resonance. It is the continuation of this initial phase-locking into a nonlinear stage that leads to excitation of autoresonant BGK modes. The amplitude of the excited electrostatic wave depends on the frequency of the drive and thus can be robustly controlled as the driving frequency varies in time.

(e) We have used our theory to show that different autoresonant waves can be excited depending on the direction of variation of the driving frequency. In the chirp-down case and sufficiently strong drive, one forms a stable relatively low amplitude excitation (the self-field amplitude a may reach several times the driving amplitude ε) involving an electron phase-space hole traversing the electron distribution as the driving

frequency decreases. In contrast, for the chirped-up case, the hole is not formed until $a \gg \varepsilon$.

(f) The autoresonant kinetic plasma waves in this study were governed by variation of parameters. In most of our examples, we used constant amplitude drives having linearly chirped frequency. Nevertheless, we have seen in both theory and simulations (see Sec. V B) that stable kinetic waves can be excited and controlled by other variations of both the driving amplitude and frequency, provided this variation is sufficiently slow. In particular, to within small modulations, the final excited wave form depends only on the final values of the varying parameters. It is this rigidity of autoresonant excitations and the insensitivity of the excited waves to the details of variation of parameters, which makes the autoresonance effect so attractive in applications.

(g) In addition to initially flat-top electron distribution, we have studied kinetic autoresonant excitations in simulations for initially Maxwellian distributions. We have observed that different autoresonant scenarios characteristic to initially flat-top distributions can be observed with Maxwellian distributions. For example, we have seen formation of autoresonant holes in phase space for chirped-down drives and excitation of large amplitude autoresonant waves for chirped-up drives. The averaged Lagrangian theory of these excitations can be developed along the lines similar to those above via a multi-water bag model as described in (c). This generalization was outside the scope of the present work, but comprises an important goal for future developments. Furthermore, it seems interesting to extend our theory to slow spatially varying plasma/drive case, as well as to include the self-consistent variation of the driving wave in the theory.

ACKNOWLEDGMENTS

This work was supported by the Israel Science Foundation (Grant No. 294/05).

APPENDIX: AVERAGED VARIATIONAL PRINCIPLE FOR DEVELOPED PHASE-SPACE HOLE PROBLEM

Similar to Sec. IV A, in the presence of the phase-space hole, we write the Lagrangian (8) as $L=L^0+L^1$, where

$$L^0 = \frac{1}{2}(\psi_{1x} - \psi_{2x} - \psi_{0x}^+ + \psi_{0x}^-)(U + U_d^0) - U + \frac{1}{2}U_x^2 - \frac{1}{4}(\psi_{1x}\psi_{1t} - \psi_{2x}\psi_{2t} - \psi_{0x}^+\psi_{0t}^+ + \psi_{0x}^-\psi_{0t}^-) - \frac{1}{12}(\psi_{1x}^3 - \psi_{2x}^3 - \psi_{0x}^{+3} + \psi_{0x}^{-3}) \quad \text{(A1)}$$

and

$$L^1 = \tfrac{1}{2}(\psi_{1x} - \psi_{2x} - \psi_{0x}^+ + \psi_{0x}^-)U^{d1}, \quad \text{(A2)}$$

where, as in Sec. IV A, $U_d^0=\varepsilon' \cos\theta \cos\Phi$ and $U_d^1=-\varepsilon' \sin\theta \sin\Phi$.

Next, we seek solutions for U, $\psi_{1,2}$, and $\psi_0^\pm$ in the form

$$U = U(\theta), \quad \psi_{1,2} = \xi_{1,2} + V_{1,2}(\theta), \quad \psi_0^\pm = \xi_0^\pm + V_0^\pm(\theta) \quad \text{(A3)}$$

where θ is the fast phase variable, $\theta_x=k$, $\theta_t=-\omega(t)$ (the slow frequency), $(\xi_{1,2})_t=-\gamma_{1,2}=0$, $(\xi_{1,2})_x=\beta_{1,2}$, $(\xi_0^\pm)_t=-\gamma_0^\pm \neq 0$, and $(\xi_0^\pm)_x=\beta_0^\pm$. Note that since $(\beta_{1,2})_t+(\gamma_{1,2})_x=0$, $\beta_{1,2}$ remain constant in time. We will assume again that the phase mismatch $\Phi=\theta^d-\theta$ is a bounded and slow function of time (this is our phase-locking assumption). We will also assume that U and V are 2π-periodic in θ and that the average $\langle U\rangle$ over θ is zero. Note also that $\beta_{1,2}=\langle v_{1,2}\rangle$, $\beta_0^\pm=\langle v_0^\pm\rangle$. These developments allow us to calculate the averaged Lagrangian by fixing all slow dependent variables and parameters in Eq. (8) at some given time and averaging over θ between 0 and 2π. The averaged Lagrangian has the form of $\bar{L}=\overline{L^0}+\overline{L^1}$, where $\overline{L^0}$ and $\overline{L^1}$ will be calculated separately. First, we substitute Eq. (A3) into Eqs. (A1) and (A2), replace $(V_{1,2})_t$ by $-u_p(V_{1,2})_x$, $(V_0^\pm)_t$ by $-u_p(V_0^\pm)_x$, and rewrite the Lagrangian (A1) as

$$L^0 = \frac{1}{2}[V_{1x} + \beta_1 - V_{2x} - \beta_2 - (V_{0x}^+ + \beta_0^+ - V_{0x}^- - \beta_0^-)](U + U_d^0) - U + \frac{1}{2}U_x^2 - \frac{1}{12}[(V_{1x}+\beta_1)^3 - (V_{2x}+\beta_2)^3 - (V_{0x}+\beta_0^+)^3 + (V_{0x}+\beta_0^-)^3] - \frac{1}{4}[-u_pV_{1x}(V_{1x}+\beta_1) + u_pV_{2x}(V_{2x}+\beta_2) + (u_pV_{0x}^+ + \gamma_0^+)(V_{0x}^+ + \beta_0^+) - (u_pV_{0x}^- + \gamma_0^-)(V_{0x}^- + \beta_0^-)] \quad \text{(A4)}$$

while

$$L^1 = \tfrac{1}{2}[V_{1x} + \beta_1 - V_{2x} - \beta_2 - (V_{0x}^+ + \beta_0^+ - V_{0x}^- - \beta_0^-)]U^{d1}. \quad \text{(A5)}$$

We again omitted terms not containing the dependent fields in Eq. (A4) as not contributing the dynamics. The problem with fixed parameters described by Eq. (A4) is integrable. Indeed, we have four conserved canonical momenta $p_{1,2}=\partial L/\partial V_{1,2x}$ and $p_0^\pm=\partial L/\partial V_{0x}^\pm$, i.e.,

$$p_1 = -\tfrac{1}{4}V_{1x}^2 + \tfrac{1}{2}(u_p-\beta_1)V_{1x} + \tfrac{1}{4}\beta_1(u_p-\beta_1) + \tfrac{1}{2}(U+U_d^0), \quad \text{(A6)}$$

$$p_2 = \tfrac{1}{4}V_{2x}^2 - \tfrac{1}{2}(u_p-\beta_2)V_{2x} - \tfrac{1}{4}\beta_2(u_p-\beta_2) - \tfrac{1}{2}(U+U_d^0), \quad \text{(A7)}$$

$$p_0^\pm = \pm\tfrac{1}{4}V_{0x}^{\pm 2} \mp \tfrac{1}{2}(u_p-\beta_0^\pm)V_{0x}^\pm \mp \tfrac{1}{4}(u_p-\beta_0^\pm)\beta_0^\pm \mp \tfrac{1}{2}(U+U_d^0) \mp \tfrac{1}{4}\gamma_0^\pm. \quad \text{(A8)}$$

These relations can be used to express V_{1x}, V_{2x}, V_{0x}^+, and V_{0x}^- in terms of $U+U^{d0}$

$$V_{1x} = u_p - \beta_1 + s_1, \quad V_{2x} = u_p - \beta_2 - s_2, \quad \text{(A9)}$$

$$V_{0x}^\pm = u_p - \beta_0^\pm \pm s_0^\pm, \quad \text{(A10)}$$

where, instead of $p_{1,2}$, $p_0^{\pm}$, we used $B_1=2p_1+(u_p/2)(u_p-\beta_1)$, $B_2=2p_2+(u_p/2)(u_p-\beta_2)$, $B_0^{\pm}=2p_0^{\pm}+(u_p/2)(u_p-\beta_0^{\pm})+\gamma_0^{\pm}/2$ and defined

$$s_{1,2}=[2(B_{1,2}+U+U_d^0)]^{1/2},\quad s_0^{\pm}=[2(B_0^{\pm}+U+U^{d0})]^{1/2}. \tag{A11}$$

In addition to $p_{1,2}$, $p_0^{\pm}$, the "energy function"

$$A=U_x^2+p_1V_{1x}+p_2V_{2x}+p_0^+V_{0x}^++p_0^-V_{0x}^--L^0 \tag{A12}$$

is also conserved in the fixed parameters case. The reduction to the integrable one degree of freedom problem is completed by substituting Eqs. (A9) and (A10) and Eq. (A4) in Eq. (A12). This yields the standard "energy" conservation law for variable U involving an effective potential

$$\tfrac{1}{2}U_x^2+V_{\mathrm{eff}}=A', \tag{A13}$$

where

$$\begin{aligned}V_{\mathrm{eff}}=&\frac{1}{4}u_p^2(-\beta_1+\beta_2+\beta_0^+-\beta_0^-)+\frac{u_p}{4}(\beta_1^2-\beta_2^2-\beta_0^{+2}+\beta_0^{-2})\\&-\frac{1}{2}(u_p-\beta_1)B_1+\frac{1}{2}(u_p-\beta_2)B_2+\frac{1}{2}(u_p-\beta_0^+)B_0^+\\&-\frac{1}{2}(u_p-\beta_0^-)B_0^--\frac{1}{6}(s_1^3+s_2^3-s_0^{+3}-s_0^{-3})+(U+U_d^0)\\&+\frac{1}{4}(\beta_0^+\gamma_0^+-\beta_0^-\gamma_0^-)\end{aligned} \tag{A14}$$

and $A'=A+1/6$. Finally, we assume a near harmonicity of U, i.e., set $U\approx a_1'\cos\theta$ (neglecting the second and higher harmonics) and use the amplitude a_1 as a new dependent variable instead of A. To this end, we average in Eq. (A13), to get

$$\begin{aligned}A'=&\frac{1}{2}\langle U_x^2\rangle+\frac{1}{4}u_p^2(-\beta_1+\beta_2+\beta_0^+-\beta_0^-)+\frac{u_p}{4}(\beta_1^2-\beta_2^2-\beta_0^{+2}\\&+\beta_0^{-2})-\frac{1}{2}(u_p-\beta_1)B_1+\frac{1}{2}(u_p-\beta_2)B_2+\frac{1}{2}(u_p-\beta_0^+)B_0^+\\&-\frac{1}{2}(u_p-\beta_0^-)B_0^--\frac{1}{6}(\langle s_1^3\rangle+\langle s_2^3\rangle-\langle s_0^{+3}\rangle-\langle s_0^{-3}\rangle)\\&+\frac{1}{4}\langle\beta_0^+\gamma_0^+-\beta_0^-\gamma_0^-\rangle\end{aligned} \tag{A15}$$

which, after the substitution in Eq. (A12) and use of $\langle U_x^2\rangle=\frac{1}{2}a_1^2$, yields the averaged Lagrangian (39) presented in Sec. IV B.

[1] T. Tajima and J. M. Dawson, Phys. Rev. Lett. **43**, 267 (1979); T. Katsouleas and J. M. Dawson, *ibid.* **51**, 392 (1983).
[2] V. M. Malkin, Yu. A. Tsidulko, and N. J. Fisch, Phys. Rev. Lett. **85**, 4068 (2000).
[3] A. Trivelpiece and R. Gould, J. Appl. Phys. **30**, 1784 (1959).
[4] L. D. Landau, J. Phys. (USSR) **10**, 25 (1946).
[5] I. B. Bernstein, J. M. Greene, and M. D. Kruskal, Phys. Rev. **108**, 546 (1957).
[6] T. O'Neil, Phys. Fluids **8**, 2255 (1965).
[7] C. B. Wharton, J. Malmberg, and T. O'Neil, Phys. Fluids **11**, 1761 (1968).
[8] K. Saeki, P. Michelsen, H. P. Pecseli, and J. J. Rasmussen, Phys. Rev. Lett. **42**, 501 (1979).
[9] J. R. Danielson, F. Anderegg, and C. F. Driscoll, Phys. Rev. Lett. **92**, 245003 (2004).
[10] H. L. Berk, C. E. Nielsen, and K. V. Roberts, Phys. Fluids **13**, 980 (1970).
[11] H. L. Berk, B. N. Breizman, J. Candy, M. Pekker, and N. V. Petviashvilli, Phys. Plasmas **6**, 3102 (1999).
[12] W. Bertsche, J. Fajans, and L. Friedland, Phys. Rev. Lett. **91**, 265003 (2003).
[13] L. Friedland, F. Peinetti, W. Bertsche, J. Fajans, and J. Wurtele, Phys. Plasmas **11**, 4305 (2004).
[14] F. Peinetti, W. Bertsche, J. Fajans, J. Wurtele, and L. Friedland, Phys. Plasmas **12**, 062112 (2005).
[15] L. Friedland, P. Khain, and A. G. Shagalov, Phys. Rev. Lett. **96**, 225001 (2006).
[16] P. Khain and L. Friedland, Phys. Plasmas **14**, 082110 (2007).
[17] G. B. Whitham, *Linear and Nonlinear Waves* (Wiley, New York, 1974).
[18] L. Friedland, Phys. Rev. E **55**, 1929 (1997).
[19] L. Friedland, Phys. Plasmas **5**, 645 (1998).
[20] C. Canuto, M. Y. Hussaini, A. Quarteroni, and T. A. Zang, *Spectral Methods in Fluid Dynamics* (Springer-Verlag, New York, 1988).
[21] P. F. Schmit and N. J. Fisch, Phys. Plasmas **17**, 013105 (2010).
[22] L. Friedland, Scholarpedia J. **4**, 5473 (2009).